THE ROLE OF OPERATIONAL VARIABILITY ON THE NON-IDEAL FLOW IN SUPERSONIC TURBINES FOR SUPERCRITICAL ORGANIC RANKINE CYCLES

Alessandro Romei[1], Davide Vimercati[2], Alberto Guardone[2], Giacomo Persico[1*]

[1] Department of Energy, Politecnico di Milano
Via Lambruschini, 4, 20156, Milano, Italy
*giacomo.persico@polimi.it

[2] Department of Aerospace Science and Technology, Politecnico di Milano
Via La Masa 34, 20156, Milano, Italy

ABSTRACT

The potential efficiency gain in supercritical Organic Rankine Cycles (ORC) must face an increase of complexity in the fluid-dynamic design of the first nozzle cascade, as severe non-ideal gas effects may possibly occur. Examples of these non-ideal effects are a non-monotonic variation of the Mach number along isentropic expansions, oblique shocks featuring an increase of the Mach number and a significant dependence of the flow field on the thermodynamic conditions at the turbine inlet.

In this work, two uncertainty-propagation scenarios, targeting the field operational variabilities, are analysed for representative first-stage nozzle cascades, whose expansion processes occur in the so-called non-ideal gasdynamic regime ($0 < \Gamma < 1$, where Γ is the fundamental derivative of gasdynamic). Realistic variabilities, derived from field measurements in running ORC power plants, are propagated through a turbulent compressible flow solver featuring generalised thermodynamic treatment via non-intrusive Polynomial Chaos representations to compare the cascade performance when Γ is either $\lesssim 1$ or $\ll 1$.

The analysis of cascade-loss distributions indicates that the considerable dependence of the flow field on the upstream total conditions induces different cascade operations from a stochastic perspective. Given uncertainties of $\approx 1\%$ in cycle design conditions, the turbine cascade operating with $\Gamma \ll 1$ exhibits cascade-loss variations as high as ± 0.75%pts with respect to the mean value, compared to approximately ± 0.15%pts when $\Gamma \lesssim 1$. Finally, the decomposition of variance contributions reveals that the most influencing parameter on the turbine performance migrates from the expansion ratio to the upstream total temperature when approaching supercritical conditions characterised by $\Gamma \ll 1$. This finding suggests that, when devising supercritical ORCs, a realistic estimate of the heat-load variability during plant operations should be taken into account in the early stage of the turbomachinery design.

1. INTRODUCTION

The ambition to exploit the efficiency gain provided by supercritical organic Rankine cycles (ORCs) (Schuster et al., 2010) has to deal with the design of turbines featuring low values of Γ, where Γ is the fundamental derivative of gasdynamic (Thompson, 1971). For these thermodynamic conditions, several non-ideal gas effects may possibly arise, e.g. a non-monotonic variation of the Mach number along isentropic expansions (Cramer and Best, 1991) and oblique shocks producing an increase of the Mach number (Vimercati et al., 2018). The usual tendency is to claim the thermodynamic advantages of the supercritical cycle layout over its subcritical counterpart, neglecting the implications of non-ideal effects on the turbine performances and operations. This works provides some numerical evidences of the change in the turbine-cascade behaviour that might occur in supercritical ORCs based on the degree of non-ideality of the flow field. The analysis is limited to supersonic first-stage nozzle cascades, which usually bear the largest pressure ratio and operate in the most severe non-ideal conditions. An uncertainty-quantification

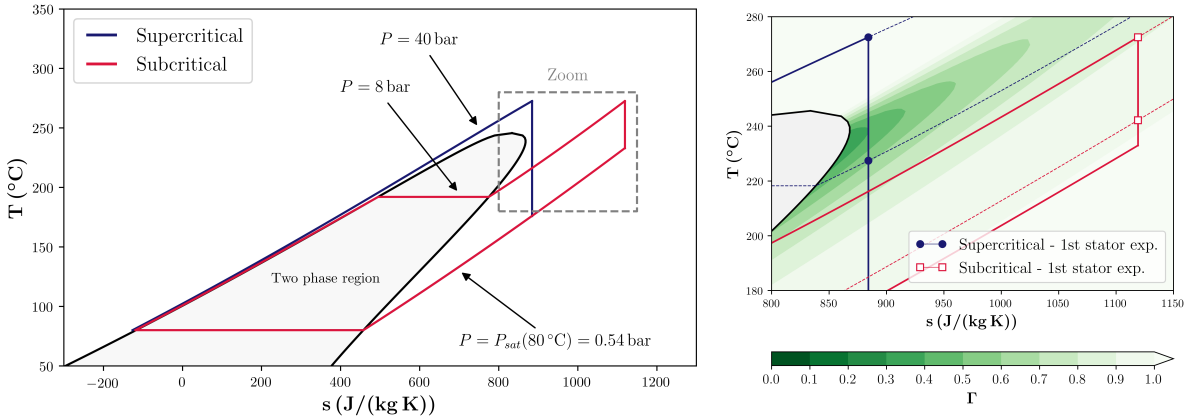

Figure 1: Representative subcritical and supercritical organic Rankine cycles with MM as working fluid. The analysis is restricted to the first-stator expansion process, which occurs within the non-ideal gasdynamic regime ($\Gamma < 1$ along the expansion).

(UQ) strategy, devised to propagate input variabilities to cascade performances, clearly reveals substantial differences in the flow evolution against small variations in the design conditions between the so-defined ideal-like operating regime ($\Gamma \lesssim 1$ along the supersonic expansion) and the non-ideal operating regime ($\Gamma \ll 1$ along the supersonic expansion). Finally, the new insight into turbines operating in the non-ideal regime allows to draw recommendations for the modelling and for the operations of future supercritical ORCs.

2. PROBLEM DEFINITION

Two ORCs are considered as references in the derivation of turbine operating conditions, namely the subcritical and the supercritical cycles reported in Fig. 1. The subcritical cycle was originally proposed by Colonna et al. (2008) for a combined heat and power application, employing the siloxane MDM (octamethyltrisiloxane, $C_8H_{24}O_2Si_3$) as working fluid. In spite of the higher saturation pressure at the condensation temperature, the siloxane MM (hexamethyldisiloxane, $C_6H_{18}OSi_2$) is considered here because it may exhibit non-ideal gasdynamic effects for temperature levels below its thermal-stability limit (Keulen et al., 2018). Moreover, both siloxanes are currently employed in combined heat and power applications (Colonna et al., 2015), thus preserving the technological relevance of following outcomes regardless of the selected fluid. The maximum temperature, which in turn corresponds to the temperature at the first-stator inlet, is set to $T_{max} = 272.5\,°C$ for both cycles. The maximum pressure for the supercritical layout ($P_{max} = 40\,bar$) offers the opportunity to achieve very low values of $\Gamma = 0.3 \div 0.4$ along the expansion process while retaining a conservative margin from the two-phase region. The outlet turbine pressure, corresponding to the saturation condition at the condensator temperature, is set to 0.54 bar for both cycles.

As previously anticipated, the analysis is limited to the first-stage nozzle cascade. Given the cycle expansion ratio, the first-stator expansion ratio depends on the number of stages arranged in the turbine and their specific reaction degrees. The number of stages is obtained by considering axial-flow turbines designed with the following rationale (Persico and Pini, 2017): the first stage provides the highest enthalpy drop ($\chi \leq 0.25$, where $\chi = \Delta h_{is}^R / \Delta h_{is}^{st}$ is the isentropic reaction degree and Δh_{is}^R, Δh_{is}^{st} are the isentropic enthalpy drop across the rotor and the stage, respectively), while the remaining stages operate at the maximum efficiency point ($\chi \approx 0.5$). This approach results in a single-stage turbine for the subcritical cycle and in a five-stage turbine for the supercritical cycle. The resulting outlet first-stator pressures are $P_1 = 1.07\,bar$ and $P_1 = 12.5\,bar$ for the subcritical and the supercritical cycle, respectively. The first-stator expansion processes are reported in the zoom of Fig. 1, where iso-Γ curves are illustrated as

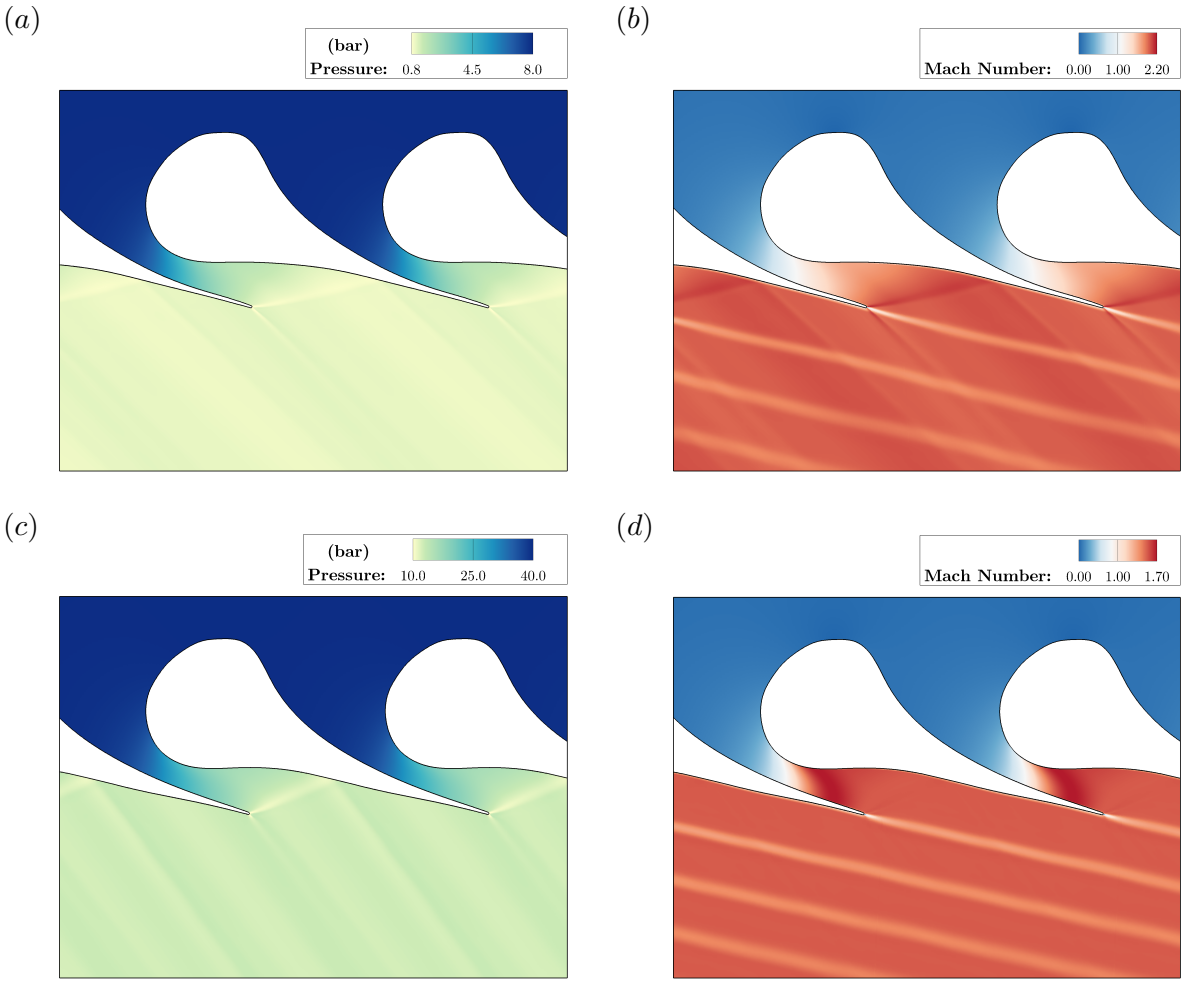

Figure 2: Pressure and Mach number fields for the nozzle cascades operating in the ideal-like (*a*-*b*) and non-ideal (*c*-*d*) operating regimes.

well. A distinction based on the value of Γ is made hereinafter: we classify the operating conditions as *ideal-like operating regime* whenever $\Gamma \lesssim 1$ in the supersonic expansion, while $\Gamma \ll 1$ in the supersonic expansion identifies the *non-ideal operating regime*. For convenience, we will refer to turbine cascades operating in the ideal-like and in the non-ideal operating regime as *ideal-like cascade* and *non-ideal cascade*, respectively. The pressure and Mach number flow fields for the two representative cascades, obtained with the numerical settings detailed in the next section, are reported in Fig. 2. Notice that, despite the smaller expansion ratio of the non-ideal cascade (β = 3.2) with respect to the ideal-like one (β = 7.5), converging-diverging profiles are adopted for both the cascades to properly accomplish the high Mach number ($M_{max} \approx 1.7$). The blade profiles for the two conditions are designed using the in-house surrogate-based shape-optimisation tool (Persico et al. (2019)). Upon inspection of Fig. 2(*d*), a non-monotonic variation of the Mach number is observed, with the local minimum Mach number located at the blade outlet. A possible advantage deriving from this condition is the enhanced uniformity of the Mach number distribution within the stator-rotor axial gap, due to the reduced sensitivity of the Mach number to perturbations in the pressure field.

Finally, as the objective of this work is to analyse the nozzle-cascade performances in field operations, the variability in the design conditions must be properly addressed. Only variabilities in the flow boundary conditions, namely inlet total temperature and total pressure and outlet static pressure, are included. The variability in the inlet flow direction and in the turbulent boundary conditions are not considered because they are negligible if compared to the contribution of operating variabilities (Romei et al., 2019).

Table 1: Uncertainties accounted in this work along with their assumed distributions ($\mathcal{U}$: uniform distribution, $\mathcal{B}$: beta distribution; $\mathcal{N}$: normal distribution, μ, σ: mean and standard deviation of the normal distribution, α, β: shape parameters of the beta distribution). For each case (i.e. ideal-like and non-ideal), two comparative UQ analyses are performed, assuming either conservative (Cons.) or more realistic (Real.) distributions based on the data available in Zanellato et al. (2018).

Uncertainty	Ideal-like, Cons.	Ideal-like, Real.	Non-ideal, Cons.	Non-ideal, Real.
T_{T0} (°C) ~	$\mathcal{U}$ on $[269.0, 276.0]$	$\mathcal{N}(\mu = 272.5, \sigma = 1.2)$	$\mathcal{U}$ on $[269.0, 276.0]$	$\mathcal{N}(\mu = 272.5, \sigma = 1.2)$
P_{T0} (bar) ~	$\mathcal{U}$ on $[7.9, 8.1]$	$\mathcal{B}(\alpha = 2, \beta = 4.5)$ on $[7.9, 8.1]$	$\mathcal{U}$ on $[39.5, 40.5]$	$\mathcal{B}(\alpha = 2, \beta = 4.5)$ on $[39.5, 40.5]$
P_1 (bar) ~	$\mathcal{U}$ on $[1.055, 1.095]$	$\mathcal{N}(\mu = 1.075, \sigma = 0.007)$	$\mathcal{U}$ on $[12.400, 12.600]$	$\mathcal{N}(\mu = 12.500, \sigma = 0.024)$

Field measurements of temperature and pressure at the outlet of the evaporator (T_{eva}, P_{eva}) and of the temperature in the condenser (T_{cond}) are reported in Zanellato et al. (2018) for running ORC power plants. Despite the power cycles are considerably different from those employed in this work, a similar relative variability can be expected. Moreover, the additional information reported along with measurements, such as time series and box-plots, can be elaborated to obtain a more adequate stochastic characterisation of input variabilities. On the basis of the available data, two kinds of stochastic characterisation can be proposed and are investigated separately in this work: (i) a conservative approach (*Cons.*) consisting in all uniform distributions, having as support the maximum relative variability, namely $\Delta T_{eva}/T_{eva} \approx 1.25\%$,$\Delta P_{eva}/P_{eva} \approx 1.25\%$, $\Delta T_{cond}/T_{cond} \approx 1\%$ with temperatures expressed in degrees Celsius; (ii) a more realistic (*Real.*) characterisation, assuming temperature measurements normally distributed and fitting the outlet evaporator pressure measurements with a beta distribution. For both scenarios, random variables are assumed to be independently distributed. Whilst outlet evaporator pressure and temperature can be directly prescribed as boundary conditions at the inlet of the turbine, the variability in the condensation temperature must be propagated to the first-stator outlet pressure. Assuming that $\Delta T_{cond}/T_{cond} = 1\%$ accordingly to what reported in Zanellato et al. (2018), a sampling strategy is applied to the machine layout and working fluid here employed to estimate the first-stator outlet-pressure variabilities (assuming constant ratios between the isentropic enthalpy drops among the blade rows during the process). A complete summary of operating variabilities considered in this work is reported in Tab. 1.

2.1 Computational flow model

Flow simulations are carried out with ANSYS-CFX 18.1®. Total pressure and total temperature (P_0^t, T_0^t) are set as inlet boundary conditions. Axial flow is prescribed at the inlet section. At the outlet, an average static pressure P_1 is imposed, accepting local pressure differences of 5%. Moreover, the outlet domain is placed approximately at four axial chords downstream of the trailing edge to avoid spurious pressure wave reflections. Since only blade-to-blade effects are of interest, quasi-three-dimensional simulations are carried out by considering a straight stream-tube around the midspan. The employed turbulence model is $k-\omega$ SST, whose inlet boundary conditions are set as Turbulence Intensity equal to 5% and eddy-to-molecular viscosity ratio equal to 10 for all simulations. The cascade Reynolds number, based on the massflow-averaged kinematic viscosity and velocity evaluated at the blade outlet and on the blade chord, is high enough ($Re = 10^7 \div 10^8$) to assume fully-turbulent flow in all simulations. The thermodynamic model used is the Span-Wagner equation of state by Thol et al. (2016), implemented as a Look-up-Tables. Thermodynamic tables are built by referring to the NIST REFPROP® database (Lemmon et al., 2013). High-resolution schemes are employed in the discretization of both flow and turbulence equations. Computations are performed on structured hexahedral meshes. A proper cell clustering near blade walls is imposed to ensure $y^+ \lesssim 1$, thus avoiding the introduction of wall functions in the solution. The grid-convergence assessment is reported in Fig. 3(a) for the two cascade configurations. For the following UQ analyses, the grid size with 200k elements in the blade-to-blade plane is chosen for both cases.

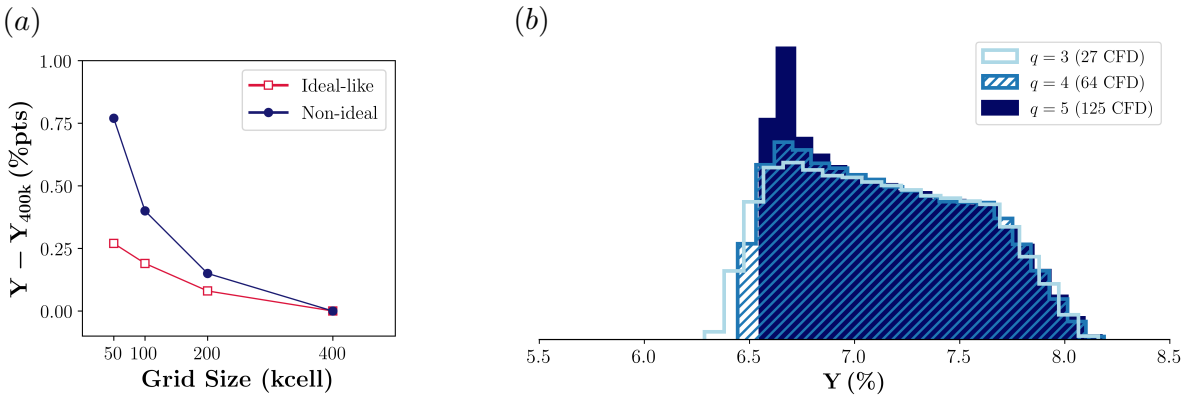

Figure 3: Computational tool assessment in terms of (*a*) grid convergence for CFD calculations (grid size refers to the mesh on the blade-to-blade surface) and of (*b*) statistic convergence for PC inference. The statistic convergence is assessed on the non-ideal cascade assuming conservative input uncertainties.

2.2 Uncertainty quantification strategy

A Polynomial Chaos (PC) expansion (Le Maître and Knio, 2012) is used as a surrogate model of the cascade total-pressure loss coefficient $Y = (P_0^t - P_{2c_{ax}}^t)/(P_0^t - P_{2c_{ax}})$, where the subscript $2c_{ax}$ indicates the section placed 2 axial chord downstream of the trailing edge, with respect to the input variabilities, namely T_0^t, P_0^t and P_1. The polynomial chaos representation allows to express a random variable, in this case the cascade loss Y, in a series of polynomials ψ mutually orthogonal to the probability measure ρ associated to the input uncertainties. For standard probability measures, such as uniform, normal and beta distributions, ψ are chosen in according to the Askey scheme (Askey and Wilson, 1985), resulting in Legendre, Hermite and Jacobi polynomials, respectively. The implemented surrogate model can be then summarised by the following expressions:

$$Y(T_0^t, P_0^t, P_1) = \sum_{i=0}^{p}\sum_{j=0}^{p}\sum_{k=0}^{p} \beta_{ijk}\psi_i(T_0^t)\psi_j(P_0^t)\psi_k(P_1) \tag{1}$$

$$\beta_{ijk} = \frac{1}{\langle \psi_i\psi_j\psi_k, \psi_i\psi_j\psi_k \rangle} \int_{\Xi} Y\psi_i\psi_j\psi_k d\rho_i d\rho_j d\rho_k \tag{2}$$

where, for the ease of readability, in Eq. (2) i, j, k indicate both the polynomial order p and the uncertainties which polynomials and probability measures refer to. The operator $\langle \cdot, \cdot \rangle$ indicates the inner product in the space $L^2(\Xi, \boldsymbol{\rho})$, where Ξ is the support of the probability density $\boldsymbol{\rho} = \rho(T_0^t)\rho(P_0^t)\rho(P_1)$, see Tab. 1. The integrals to determine the polynomial chaos coefficients β_{ijk} is solved by tensorization of the corresponding Gaussian quadrature rule of order q in each stochastic dimension, resulting in q^3 CFD evaluations. Each polynomial order is truncated at the order $p = q - 1$. Once the PC representation is determined, statistics are computed by sampling the surrogate model, which is much cheaper in terms of function evaluation. Three quadrature orders are investigated in terms of cascade-loss distributions for the non-ideal case featuring conservative uncertainties in Fig. 3(*b*). The distributions, along with their main statistical moments, are very similar for the three quadrature orders, slightly differing only for the low quantiles. Then, $q = 4$ is used for the following studies. Total Sobol indices, which stems from the variance decomposition and quantify the global impact of each uncertainty to the cascade-loss, are computed directly from the PC coefficients β_{ijk} (Crestaux et al., 2009).

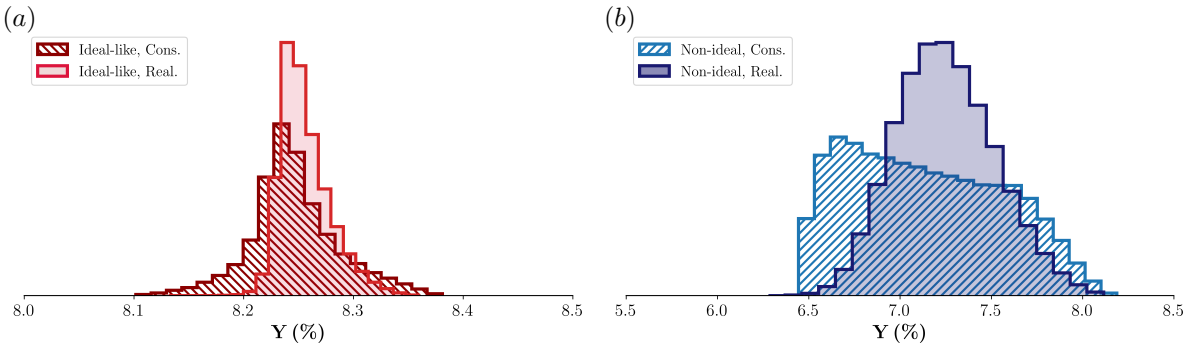

Figure 4: Probability density distributions for the cascade loss coefficient in the ideal-like (*a*) and non-ideal (*b*) operating regimes, considering both conservative and realistic input uncertainties.

3. FIELD PERFORMANCE OF SUPERSONIC NOZZLE CASCADES

The probability distributions for the four stochastic problems of Tab. 1 are reported in Fig. 4. First, the two stochastic characterisations are compared. As expected, the conservative approach predicts higher probabilities to extreme values compared to the realistic counterpart, although similar distribution supports are found. In the present case, the maximum range of variation is of primary interest, as it is not possible to directly compare the cascade performances from a probabilistic perspective. On the other hand, the deviation from the nominal performance relatively to each cascade can be properly compared, as the variabilities are consistently computed for the two cases. Regardless of the stochastic characterisation, which in this case provides marginal discrepancies in terms of distribution supports, the ideal-like cascade shows a maximum variation with respect to the mean value as low as ±0.15%pts; on the contrary, the non-ideal cascade exhibits a variation up to ±0.75%pts. As a result, given the same cycle variabilities, the non-ideal cascade performance changes more than the ideal-like counterpart, featuring approximately five-time larger variations.

The peculiar response to operational variabilities has a clear physical explanation. Referring to Fig. 5, which reports the coefficient-of-variation fields $CoV = \sigma/\mu$, where μ and σ are the mean and the standard deviation, respectively, for the pressure and the Mach number, the two cascades feature a distinct flow evolution under uncertainties. Regardless of the stochastic characterisation, the ideal-like case exhibits slight variations only in the oblique-shock patterns downstream of the trailing edge. On the other hand, the non-ideal cascade shows considerable uncertainties even in the expansion process occurring within in the blade channel, which in turn affect the expansion in the rear part and eventually the formation of shock waves. This marks the high sensitivity of the so-called non-ideal effects to relatively small variations in the operating conditions, thus indicating the relevance of a systematic analysis of the expected operational variability when designing the turbine for supercritical ORCs.

A classification of the variability impact on the cascade performance can help to understand these differences in the flow evolution. Figure 6 reports a sensitivity analysis based on total Sobol indices $S^T(Y)$, which quantify the contribution of each uncertainty to the total variance of the cascade performance. For the ideal-like cascade, the expansion process is almost entirely determined by the expansion ratio, as the higher contributions of the pressure upstream and downstream of the cascade highlight. This result agrees with the predictions of the isentropic theory. If the expansion ratio varies, the flow must adjust downstream to match the prescribed expansion process, resulting in different oblique-shock/post-expansion patterns downstream of the trailing edge. The non-ideal case, instead, is completely dominated by a variation in the upstream total temperature. Indeed, in non-ideal flows ($\Gamma < 1$), the expansion process also depends on the upstream thermodynamic states. This additional contribution to the expansion process, which is negligible in the ideal-like operating regime, overcomes the contribution given by a variation in the expansion ratio. As a result of a change in the total temperature, the adapted expansion process

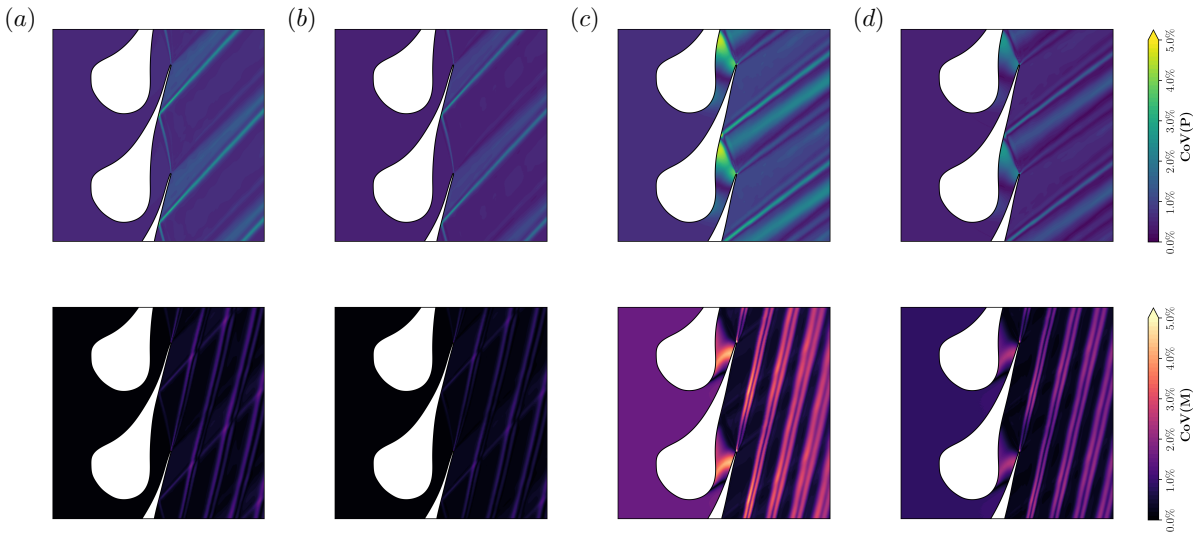

Figure 5: Pressure and Mach number CoV fields for (*a*) ideal-like cascade and conservative input uncertainties, (*b*) ideal-like cascade and realistic input uncertainties, (*c*) non-ideal cascade and conservative input uncertainties, and (*d*) non-ideal cascade and realistic input uncertainties.

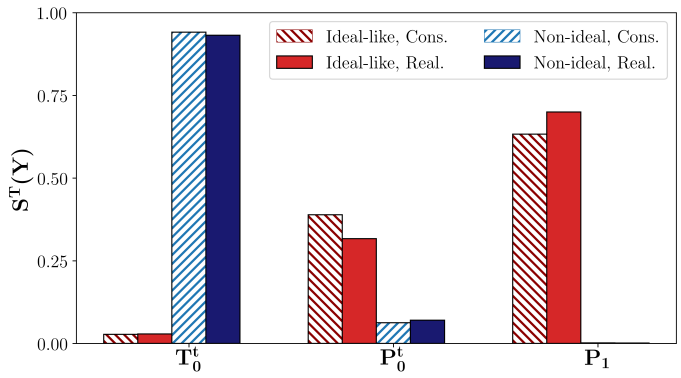

Figure 6: Total Sobol indices of the cascade loss coefficient for the four stochastic problems.

changes as well; then, since the expansion ratio within the blade channel is prescribed by the nozzle-cascade shape, the flow has to adjust downstream to match the outlet pressure, thus generating stronger shocks/expansion fans downstream of the cascade. Notice that, although a variation in the shock pattern can be appreciated in the CoV-pressure field downstream of the non-ideal cascade, the corresponding CoV-Mach-number field displays only peaks in the wake uncertainties, preserving the averaged Mach number despite the shock modification. The highest CoV of Mach number is found, in fact, within the bladed region upstream of the cascade opening; this is another effect of non-ideality. As a matter of fact, the Mach number distribution exhibits a non-monotone trend in the divergent downstream of the throat; such trend, which is a typical non-ideal feature, is determined by the inlet conditions, and hence it is strongly altered by their variations.

From the cycle operational perspective, the significant dependence of the non-ideal cascade flow field and performance on the temperature at the evaporator outlet suggests that heat-load variability has to be either minimised to keep the turbine working at high efficiency or directly accounted for in the turbine design process. Moreover, as it is impossible to completely remove operational variabilities, the larger cascade performance variations must be properly acknowledged when subcritical and supercritical cycles are compared.

4. CONCLUSIONS

When dealing with supercritical organic Rankine cycles, the first stages of the turbine may operate in thermodynamic regions featuring very low values of Γ. Since this parameter has a great influence on the gasdynamic evolution of the expansion process, it is expected to have an impact on the turbine performance as well. The results shown in this paper confirms this expectation by means of a numerical comparison between two representative first-stator supersonic nozzle cascades, whose expansion processes are characterised by $\Gamma \lesssim 1$ and $\Gamma \ll 1$, respectively. The cascade operating in the regime $\Gamma \ll 1$ features a non-monotonic trend in the Mach number along the expansion process, producing a highly uniform Mach number field downstream of the cascade trailing edge. Operating variabilities, deduced by field measurements in currently running ORC power plants, are reformulated in stochastic terms considering both a conservative (i.e., less refined) and a realistic approach, and are propagated through an uncertainty-quantification strategy based on the Polynomial Chaos expansion to derive the cascade-loss distribution. In this way, the inherent variabilities in the design conditions are properly accounted for when the two cascades are compared. The analysis of the maximum variations in cascade-loss distributions reveals that, given the same relative uncertainties in the corresponding power cycles, the cascade performance admits a variation of $\pm 0.15\%$pts and $\pm 0.75\%$pts for $\Gamma \lesssim 1$ and $\Gamma \ll 1$, respectively. The use of a conservative approach in formulating the input uncertainties in spite of a more realistic one leads to only marginal differences in the performance variability. The resulting five-time larger variations in the cascade performance when $\Gamma \ll 1$ is attributed to the significant dependence of the flow field and of the expansion process on the upstream total temperature, which is approximately negligible when $\Gamma \lesssim 1$. This peculiar turbine behaviour should be properly addressed when supercritical ORCs are devised.

REFERENCES

Askey, B. K. and Wilson, J. (1985). *Some Basic Hypergeometric Orthogonal Polynomials that Generalize Jacobi Polynomials*. American Mathematical Society.

Colonna, P., Casati, E., Trapp, C., Mathijssen, T., Larjola, J., Turunen-Saaresti, T., and Uusitalo, A. (2015). Organic Rankine Cycle power systems: From the concept to current technology, applications, and an outlook to the future. *J. Eng. Gas Turb. Power*, 137(10):100801–1–19.

Colonna, P., Harinck, J., Rebay, S., and Guardone, A. (2008). Real-gas effects in organic rankine cycle turbine nozzles. *J. Propul. Power*, 24(2):282–294.

Cramer, M. S. and Best, L. M. (1991). Steady, isentropic flows of dense gases. *Phys. Fluids A*, 3(4):219–226.

Crestaux, T., Le Maître, O., and Martinez, J. M. (2009). Polynomial chaos expansion for sensitivity analysis. *Reliability Engineering and System Safety*, 94(7):1161 – 1172.

Keulen, L., Gallarini, S., Landolina, C., Spinelli, A., Iora, P., Invernizzi, C., Lietti, L., and Guardone, A. (2018). Thermal stability of hexamethyldisiloxane and octamethyltrisiloxane. *Energy*, 165:868 – 876.

Le Maître, O. and Knio, O. M. (2012). *Spectral Methods for Uncertainty Quantification: With Applications to Computational Fluid Dynamics*. Scientific Computation. Springer Netherlands.

Lemmon, E. W., Huber, M. L., and McLinden, M. O. (2013). NIST reference database 23: reference fluid thermodynamic and transport properties–REFPROP, version 9.1. *Standard Reference Data Program*.

Persico, G. and Pini, M. (2017). 8 - Fluid dynamic design of Organic Rankine Cycle turbines. In Macchi, E. and Astolfi, M., editors, *Organic Rankine Cycle (ORC) Power Systems*, pages 253 – 297. Woodhead Publishing.

Persico, G., Rodriguez-Fernandez, P., and Romei, A. (2019). High-fidelity shape-optimization of non-conventional turbomachinery by surrogate evolutionary strategies. *Journal of Turbomachinery*, 141(8):081010.

Romei, A., Congedo, P. M., and Persico, G. (2019). Assessment of deterministic shape optimizations within a stochastic framework for supersonic organic rankine cycle nozzle cascades. *Journal of Engineering for Gas Turbine and Power*, 141(7):1–11.

Schuster, A., Karellas, S., and Aumann, R. (2010). Efficiency optimization potential in supercritical organic rankine cycles. *Energy*, 35(2):1033 – 1039.

Thol, M., Dubberke, F. H., Rutkai, G., Windmann, T., Köster, A., Span, R., and Vrabec, J. (2016). Fundamental equation of state correlation for hexamethyldisiloxane based on experimental and molecular simulation data. *Fluid Phase Equilibria*, 418:133 – 151.

Thompson, P. A. (1971). A fundamental derivative in gasdynamics. *Phys. Fluids*, 14(9):1843–1849.

Vimercati, D., Gori, G., and Guardone, A. (2018). Non-ideal oblique shock waves. *J. Fluid Mech.*

Zanellato, L., Astolfi, M., Serafino, A., Rizzi, D., and Macchi, E. (2018). Field performance evaluation of geothermal ORC power plants with a focus on radial outflow turbines. *Renewable Energy*.